Research Square

Preprints are preliminary reports that have not undergone peer review.
They should not be considered conclusive, used to inform clinical practice,
or referenced by the media as validated information.

A New Empirical Model for Evaluating the Swelling Rate Behaviour of Test Data Clay Soils Containing Different Amounts of NaCl and KCl Solutions

Uri Komornik
Ariel University
David Benoliel
davidbo@ariel.ac.il
Ariel University

Research Article

Keywords: Clays, Suction, Swelling rate, Mathematical modeling, Laboratory tests

Posted Date: March 27th, 2026

DOI: https://doi.org/10.21203/rs.3.rs-9129009/v1

License: This work is licensed under a Creative Commons Attribution 4.0 International License.
Read Full License

Additional Declarations: No competing interests reported.

A New Empirical Model for Evaluating the Swelling Rate Behaviour of Test Data Clay Soils Containing Different Amounts of NaCl and KCl Solutions

Uri Komornik,[1] and David Benoliel, [1]

[1] Department of Civil Engineering, Ariel University, Science Park 3, Ariel 40700000, Israel.

Contributing authors:

uri_k@ariel.ac.il;ORCID:https//orcid.org/0000-0003-4115-309X,

Davidbo@ariel.ac.il;ORCID:https//orcid.org/0000-0002-3491-560X.

Corresponding author:

Davidbo@ariel.ac.il, ORCID:https//orcid.org/0000-0002-3491-560X.

Abstract

Sodium and Potassium Chloride are used in several places worldwide to melt snow covering the ground. The site soil section may include clayey soils that are potentially volume-changing due to variations in water content. This phenomenon can cause the uplifting and settlement of structures and roads, resulting in considerable damage. Sodium- or Potassium-Chloride solutions that penetrate the ground influence the swelling and swelling pressure of clayey soil. A new mathematical model for describing the swelling rate of clayey soils was developed from test data observations and expressed as a function of the logarithm of time. The model is divided into two different consecutive sub-models corresponding to two modes of adsorption: (i) a first mode, shorter and rapid, (ii) a second mode, longer and slower. Those two modes may be confirmed by the matric/osmotic theory of clay swelling. The two sub-models have two different mathematical expressions. The research included a comparison of the new model analysis with laboratory test results. The tests were performed using two clayey soils, Ariel and Senneck clays, containing different amounts of Sodium and Potassium Chloride solutions. For the Ariel and Senneck clays, Potassium Chloride solutions are more effective at reducing swelling than Sodium solutions. The research results demonstrate that the new model accurately represents the time-dependent swelling behavior of clayey soils under various Sodium and Potassium Chloride solutions.

Keywords: *Clays, Suction, Swelling rate, Mathematical modeling, Laboratory tests*

Introduction

Sodium Chloride, or, less frequently, Potassium Chloride, is used in several places worldwide to melt snow covering the ground. The soil section at the site may include clayey soils that are potentially volume-changing due to variations in water content. This phenomenon may cause considerable damage to structures and roads. The Penetration of Sodium or Potassium chloride into soil layers influences the swelling of clayey soils and the swelling pressure these soils exert on structures and roads.

Estimating the swelling displacement and the developed pressure of clayey soils has primarily been reported without accounting for the time-dependent swelling rate. Empirical equations were investigated to predict the final swelling behavior of compacted expansive soils, based on osmotic and mechanical phenomena [1] and to predict the swelling pressure of compacted clays [2-3]. Djedid et al. (2013) [4] presented a comparison of different models for predicting the swelling and pressure of compacted clays.

The rate of swelling that develops over time has been modeled using a rectangular hyperbolic equation [5-10]. Komornik and Benoliel [11] introduced a time-dependent parameter in the hyperbolic equation; the swelling curve was then divided into two parts. Lalji et al. 2021 [12] provided a third-degree polynomial equation scaled to swelling parameters. The time-log swelling graph is divided into three sections: initial, primary, and secondary swell [10,13-14].

The concentration of saline solutions reduces the swelling, liquid limit, and plasticity of expansive clayey soils, thereby increasing soil stability [15-21]. As the valence of the cations and the temperature of the electrolyte solutions increase, the degree of swelling decreases [15-16].

Several fundamental research studies have been conducted on the electro-microstructural formulation of water adsorption in clay soils and on the effects of electrolytes on swelling stabilization. It was proven that there are two mechanisms of adsorption of electrolytes into clays: inner crystalline (or matric) and osmotic (or DDL) [22-28]. The matric adsorption is independent of the dissolution of salt in water, and the osmotic adsorption is dependent on the concentration of salt in the solution. However, osmotic suction inhibits matric suction [27].

The influence of the cation K^+ on the reduction of swelling and the collapse of DDL adsorption during the soil clay deformation process has been observed [29-30]. Yilmaz and Marschalko (2014)[31] compared the effects of the cations Na^+ and K^+ on swelling and ion exchange during swelling: the exchange of Na+ ions is reversible, whereas that of K^+ ions is irreversible. The swelling depends on the hydrated cation's radius. The atomic radius of K^+ is bigger than that of Na^+, resulting in less swelling with electrolytes containing K^+ cations compared to those containing Na^+ cations [32]. Parameters for measuring the primary and secondary swelling rates are defined, demonstrating that the primary swelling rate is typically much faster than the secondary swelling rate [10,33-34].

A new model for estimating swelling was developed using the variable *s*, which represents the logarithm of time. The model is divided into two consecutive sub-models: (i) which involves swelling at the beginning of the process and includes innercrystalline absorption of electrolyte water into clays, and (ii) which encompasses the diffuse double layer (DDL) absorption mechanism. The research included a comparison of the new model analysis with laboratory test results. The tests were performed using two clayey soils, Ariel and Senneck clays, containing different amounts of Sodium and Potassium Chloride solutions. The new model is based on observations of laboratory test results and is supported by theoretical research published in the literature; therefore, these issues are introduced first.

2. A Brief Explanation of Clay Swelling in Pure Water and Salty Water

2.1 Electro-Chemistry of Pure Water and Salty Water

Water molecules, H_2O, are dipolar, i.e., they have positive charges on one side (the two positively polarised hydrogen atoms (H^+ and H^+) and negative charges on the other side (the negatively polarised oxygen atom (O^{2-}). A small amount of water molecules dissociates into cations (H^+) and anions (OH^-) with a concentration of 10^{-7} moles per liter, giving the *pH* of the pure water a value of seven (pH=-log$([H^+]=7$). When added to water, Sodium or Potassium chloride dissolves until a saturation concentration is reached. The salt molecules dissociate completely into cations (Na^+ or K^+) and anions (Cl^-), increasing the water's conductivity.

2.2 Electro-Chemistry of Clay

Clay minerals are complex aluminum silicates composed of two basic units: silica tetrahedra (T) and alumina octahedra (O) sheets. The clay layers are associated with T-O or T-O-T sheets and carry negative surface charges. Cations in the environment are attracted to the inter-layer space to compensate for the charge deficit and bind the clay layers through electrostatic attraction. There are three essential families of clay minerals: Kaolin, Illite, and Montmorillonite [35]. Kaolin consists of repeating layers of elemental tetrahedral-octahedral (T-O) sheets. The layers are held together by hydrogen bonding. Illite consists of a repeating layer of an octahedral sheet bonded to two tetrahedral sheets, one at the top and another at the bottom (T-O-T). Potassium ions bind the illite layers. Montmorillonite has a T-O-T layer structure. The bond between the layers is very weak, and many water molecules may be attracted into the interlayer space.

2.3 Electro-Chemistry of Clay Inundated by Water

When inundated with water, bounding cations (which bind the clay layers with varying intensities) become free. Different cations float in the clay layers, forming a Diffuse Double Layer (DDL). In the DLL layers, cation concentration decreases with increasing distance from the clay surfaces.

2.4 Clay Soils Swelling

The phenomenon of clay swelling has been explained by various authors [22-24]. According to their research, cations and the positive poles of water molecules are attracted to the interlayer spaces to compensate for the clay's electronegative surface. Additionally, the negative poles of water molecules are attracted to free cations in the diffuse double layer, thereby increasing the clay's interlayer spacing. Thus, the phenomenon of swelling can be described by two-phase mechanisms:

1) The matric (or innercrystalline or capillarity) suction is preponderant at the beginning of the swelling, also called the primary phase. It consists of the orderly attraction of several layers of dipolar water molecules to the negatively polarized clay surface layers.

2) The osmotic or diffuse double-layer suction is predominant at the end of the primary swelling process. It consists of the attraction of dipolar water molecules to free cations, away from the surface clay layer, in a diffuse manner.

According to the research mentioned above, the relative contributions of crystalline and osmotic swelling depend on the clay type, the composition of exchangeable cations, and the composition of the inundating salt solution. Water rich in cations accelerates the neutralization of negative charges on clay layers, reduces the amount of adsorbed water, and consequently leads to a more stable soil structure.

2.4.1 The Matric (or Innercrystallite, Crystalline, or Capillarity) Suction

Crystalline swelling is driven by the adsorption of water molecules, which are attracted to the negatively charged clay's interfaces. It is preponderant at the beginning of the swelling process. It primarily depends on the initial soil moisture content and is less dependent on the concentration of the cation solution. As the cation concentration increases, the matric suction phase shortens. Due to its short duration, innercrystalline suction is referred to as short-term swelling [34].

2.4.2 Osmotic/Double Layer Suction

After the completion of the crystalline swelling, the matric swell becomes negligible. Then, the diffuse double-layer (DDL) repulsion dominates the swelling, leading to the second swelling mechanism [28]. Layers of water molecules separate the clay layers from the DDL. The negative poles of the dipolar water molecules are attracted to the positively charged cations in the diffuse double layers. The osmotic swelling process develops slowly and takes considerable time to

complete. Therefore, it is also referred to as long-term swelling [34]. The diffuse double-layer repulsion mainly drives the osmotic swell phase. Osmotic swelling exhibits an almost linear relationship (in percent swelling vs. the logarithm of time) [10].

The matric mechanism of adsorption is dominant at the beginning of the process, whereas the osmotic mechanism is dominant at the end; however, the two mechanisms remain additive throughout the process [27-28].

3. Experiment Process for Obtaining Swelling Test Results

Swelling tests were performed according to ASTM D4546-08 [36] using Petro Tech distilled water and varying amounts of 99.9% pure Sodium and Potassium Chloride from Glentham Life Sciences. A 26-WF31E20 SW consolidometer apparatus (from the company "Controls") was used to perform the tests. This type of consolidometer features two sensors: one measures the vertical displacement, while the other maintains a constant vertical pressure. The pressure was applied at the beginning of each test, when the soil samples were dried, and remained constant on the specimen throughout the tests. Five test series were performed at fixed, constant vertical pressures on Ariel and Senneck clayey soils. The Ariel clayey soils were used for three series of experiments at 1 kPa and 2 kPa with different Sodium Chloride concentration solutions, and one at 1 kPa with different Potassium Chloride concentration solutions. The Senneck clay soils were used for two series of experiments at 0.1 kPa with different concentrations of Chloride and Potassium Chloride solutions. A total of twenty-eight experiments were performed.

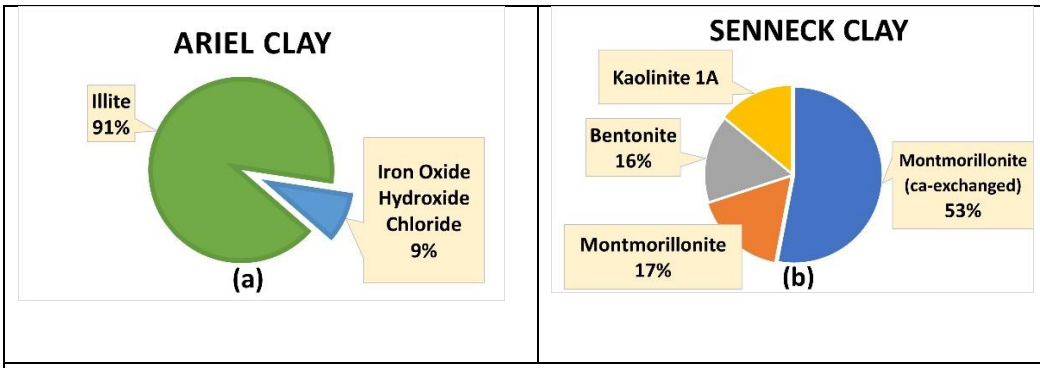


Fig. 1 Chemical Composition of the Tested Clays from XRD Analysis (**a**) Ariel Clay, (**b**) Senneck Clay

4. Description of the Soil Samples

An XRD (X-ray diffraction) analysis was performed on the Ariel and Senneck soil samples. These Ariel clay samples comprise 91% illite and 9% iron hydroxide chloride (Figure 1a). The Senneck clay samples comprise 70% montmorillonite, 16% bentonite, and 14% Kaolinite (Figure 1b). The Atterberg analysis was performed on these two clay types in accordance with ASTM D4318-17 [37]. Both clays were classified as CH (High-plasticity Clay). Table 1 summarizes the average initial properties of the soil samples at the pressure conditions of each experiment series: 1 kPa and 2 kPa for the Ariel clay, and 0.1 kPa for the Senneck clay.

	Ariel Soil		Senneck Soil
After Pre-Consolidation at	**1kPa**	**2kPa**	**0.1kPa**
Specific Gravity [-]	**2.85**	**2.85**	**2.719**
Water Content [%]	**3.41**	**3.41**	**3.51**
Plastic Limit [%]	**33**	**33**	**44**
Liquid Limit [%]	**66**	**66**	**80**
Unit Weight [kN/m^3]	**12.53**	**13.43**	**11.17**
Dry Unit Weight [kN/m^3]	**12.16**	**12.85**	**10.76**
Void Ratio [-]	**1.31**	**1.22**	**1.50**
Saturation [%]	**8**	**7.45**	**6.5**
Specimen Weight [g.]	**32.56**	**32.58**	**20.15**
Dry Specimen Weight [g.]	**31.49**	**31.51**	**19.47**

Table 1 Average Initial Characteristics and Conditions of the Ariel and Senneck Clay Samples

165

5. Preparation of Soil Samples

The soil sample was first washed through a 75-micron sieve (ASTM #200) into a large container. The large container stayed still for at least 24 hours. The mixture of silt and clay was dried in an oven at 60°C for three days. The dried mixture was crushed using a cylindrical plastic hammer and passed through a sieve with an ASTM #40 opening (425 microns) to obtain soil powder. This soil powder sample was poured into the consolidometer mold, covering an area of 20 cm^2. The upper surface was leveled using a 300-gram cylinder, which applied 1.5 kPa of pressure to the soil sample. A porous stone and a cap were placed on the top of the specimen, resulting in an additional pressure of 0.5 kPa.

6. Observation of the Swelling Data

The experimental testing included measuring the displacements of the Ariel and Senneck clay soil samples, which were exposed to Sodium and Potassium Chloride solutions at different concentrations. These test results were compared with the displacements developed using distilled water for over 24 hours.

All the data were observed on the logarithm of time, or "s," on the x-axis. Figures 2a and 2b (from series No.1 and No.2) compare the effect of the initial constant pressure condition on the Ariel-clay soil at 1 kPa and 2 kPa, respectively. Figures 3a and 3b (from series No. 1 and No. 3), and Figures 4a and 4b (from series No. 4 and No. 5) illustrate and compare the relationship between swelling using different concentrations of Sodium and Potassium Chloride solutions on the Ariel and Senneck clay soils, respectively. These Figures indicate that, in general, the swelling phenomenon has two components when expressed as a function of the logarithm of time. The first component includes both latent (initial) and rapid swelling, while the second component comprises only slow swelling. For all twenty-eight experiments, the speed and the acceleration curves were computed and plotted. Two examples of such speed and acceleration curves are shown in Figs. 5a and 5b**.**

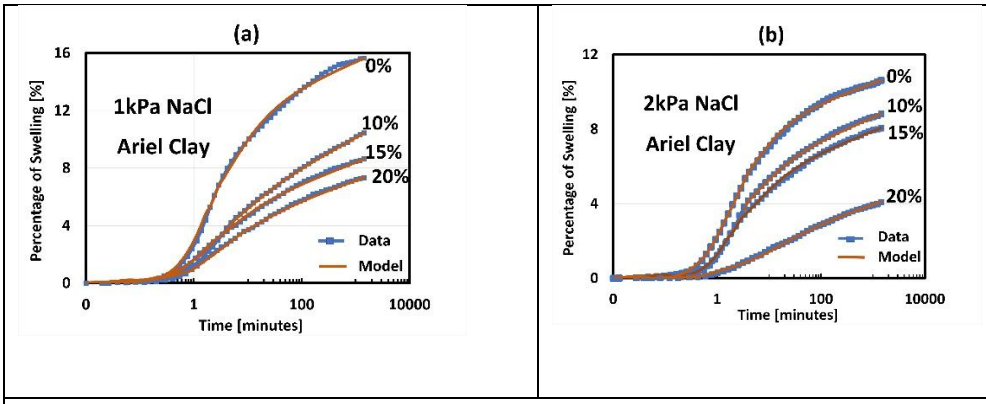


Fig. 2 Comparison of Ariel Clay Swelling at Different Initial Pressure Conditions: (**a**) 1 kPa, **(b)** 2 kPa, for Different Sodium Chloride Concentration Solutions (Test Data with New Model)

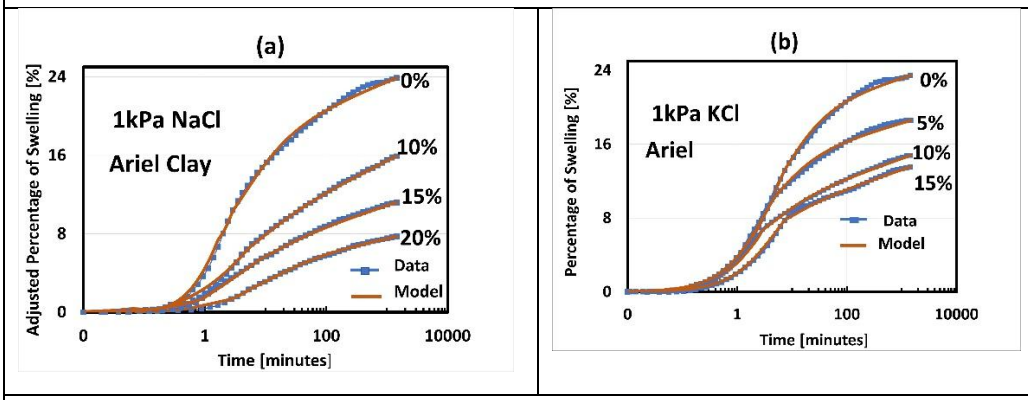


Fig. 3 Comparison of Ariel Clay Swelling at 1kPa Conditions for Different Weight Concentration Salt: (**a**) NaCl, (**b**) KCl, with the New Models

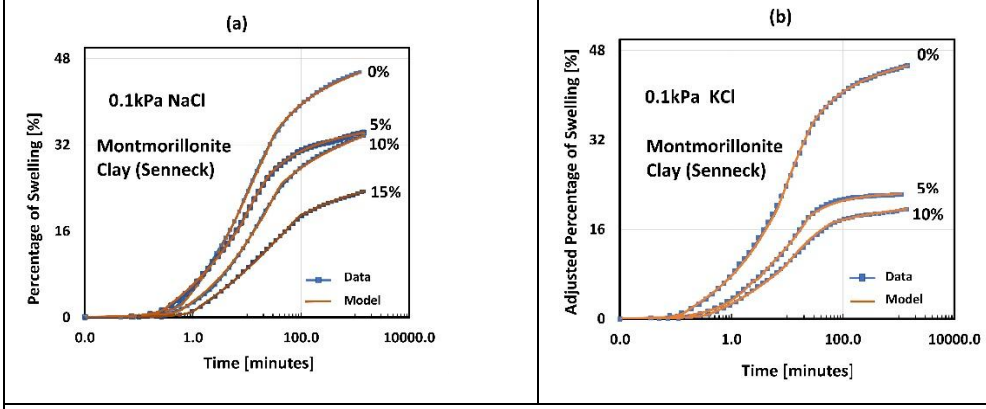


Fig. 4 Comparison of Montmorillonite Senneck clay Swelling at 0.1kPa Conditions for Different Weight Concentration Solutions: **(a)** NaCl, **(b)** KCl with New Models

191

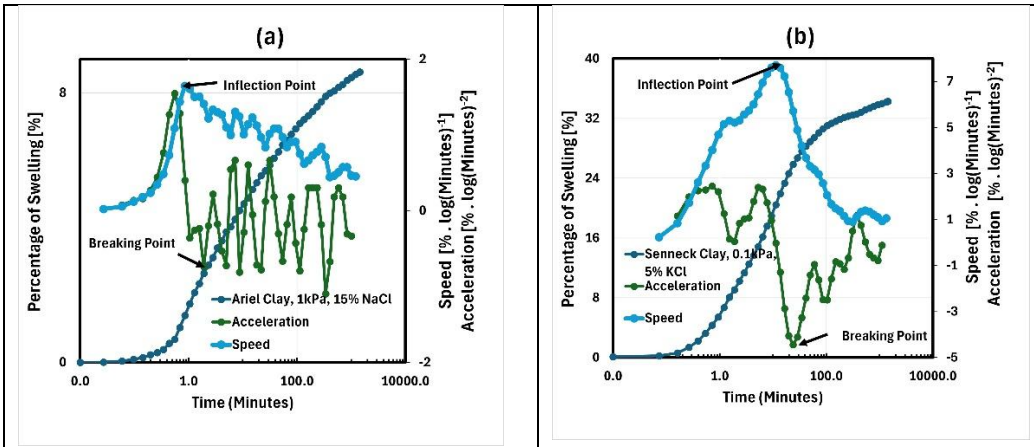


Fig 5 Two examples of Swelling (in Primary Y-axis), Speed and Acceleration Curves (in Secondary Y-Axis): (**a**) Second Mode: Linear Part Important (Cascaded Adsorption), (**b**) Second Mode: Sigmoid Part Important: Slope Break Clearly Visible

192

6.1 General Observations of the Effects of Salty Solutions on the Shape of the Swelling Curves

The following conclusions can be derived from the test results shown in Figs. 2-4:

- Using distilled water:
  - The swelling curve may be divided into three parts in the log*(t)* x-axis: a very short and rapid convex part, a longer and less rapid linear part, and a very long and slow concave part corresponding to three phases: this is the S-shape of the adsorption curve (initial, primary, and secondary swells).
- Using salty solutions:
  - The swelling rate increases until an inflection point, while conserving the beginning of the S-shape, then decreases slightly over a short period and *abruptly reaches a breaking point*, where it sharply decreases and presents an almost linear shape.
  - The beginning S-shape and the breaking point with the following almost linear shape suggest *two adsorption mechanisms* and two phases of swelling.
  - The swelling rate decreased significantly at the last stage of the swelling process.
  - The inflection point occurs before the half-swell point. The slope break suggests that a *second adsorption mechanism inhibits and shortens the first one.*
- As the salt concentration increases:
  - The point of inflection and the slope break occur earlier, and the second part of adsorption becomes more pronounced and almost linear.
  - The second part of the curve becomes less concave and more linear, and the slope break becomes more abrupt.

The experimental swelling speed and acceleration curves were plotted for all twenty-eight experiments. Two examples of the speed and acceleration curves are given in Fig. 5. The following conclusions can be drawn:

- The minimum in the acceleration curves is the exact location of the breaking point of each swelling curve.
- Beyond this minimum, the curves exhibit a succession of maxima and minima (sawtooth pattern), suggesting that the adsorption curves tend to be linear and that the adsorption phenomenon occurs in a *cascaded* manner.
- The inflection point always occurs between the highest minimum and the highest maximum of those curves at the intersection of the acceleration curve with the zero line. The inflection point is also the maximum in the speed curve.
- The more the swelling curve is linear, the more pronounced the succession of minima and maxima after the breaking point.

7. Suggested New Model for Evaluating the Swelling Clayey Soil Behaviour

The new suggested expression for the swelling model is based on observations of both the test results curves and the calculated experimental acceleration curves $\left(\frac{d^2S}{d(log(t))}\right)$, which are illustrated on a logarithmic time scale. Therefore, the models are expressed as a function of a variable "*s*", which is equal to the logarithm of time: *s* = log*(t)*. The advantage of this representation is that the characteristics of the adsorption curve, i.e., the inflection point and the breakpoint, are readily visible or calculable. The model represents a pseudo-second-order expression in the s-domain, an exponential-sigmoid function, and is more suitable for describing the swelling of clays in saline solutions. All the experimental data confirm that there are two modes of swelling, and therefore two mathematical expressions describing those two modes of swelling. The two modes of swelling occur simultaneously; however, the first mode is preponderant at the onset and lasts only briefly, whereas the second mode is preponderant at the end and persists longer. The two modes of swelling may be identified as : (i) the inner-crystalline and (ii) the osmotic parts of swelling, as described in the literature [22-24]. The first mode exhibits an S-shaped (exponential-sigmoid) profile, while the second mode becomes increasingly linear as the salt concentration in the water increases. It is assumed the first part of the swelling is exponential-sigmoid, and the second mode is linear in the s-domain, or hyperbolic and logarithmic in the time domain, respectively. The limit between the preponderant first mode and the preponderant second mode is the slope break observed in the swelling curve, or in the acceleration curve, expressed by a strong minimum. Because the sigmoid-exponential is a model going from $-\infty$ *to* $+\infty$, the model is restricted between a *s*-starting and an *s*-ending points, taking as: $s_{start} = log(0.1)$ and $s_{\mathrm{end}} = log(t_{end})$. The value s_{start}, is when the clay swelling begins at time 0.1 minutes, and s_{end} is the value when it ends at the ending time t_{end} This model is not a pure translation of the time domain into the $\log(t)$ domain, but constitutes a new model. There is no swelling value of zero for the model expressed in the s-domain, while there is a swelling value of zero for the model expressed in the time domain. The two-equation sub-models can be written as follows:

1) For the first mode of the adsortion equation, $S_1(s)$, starting at the beginning of the experiment and ending at the breaking point, is given by the following three equations:

$$S_{11}(s)[\%] = S_f \frac{e^s}{C_1 + e^s} \qquad s \in [s_{start}, s_{break}] \qquad (1)$$

Sometimes, the second mode of swelling is additive, sometimes it is subtractive [27]; therefore, equation 1 may be pondered by the following linear function:

$$S_{12}(s) = C_{11} + C_{12}\, s \qquad s \in [s_1, s_2] \qquad (2)$$

s_1 and s_2 are the locations where the corrections are necessary.

The total first mode equation, $S_1(\mathrm{s})$, may be a combination of equations (1) and (2):

$$S_1(s) = w_1 S_{11} + (1 - w_1) S_{12} \qquad s \in [s_{start}, s_{break}], \quad (3)$$

$$w_1 \in [0,1]$$

2) For the osmotic suction $S_2(s)$ equation, starting at the breaking point until the end of the experiment, is given by the following three equations:

$$S_{21}(s)[\%] = S_f \frac{e^s}{C_1 + e^s} \qquad s \in [s_{break}, s_{end}] \quad (4)$$

The following linear equation ponders equation 4:

$$S_{22}(s) = C_{21} + C_{22} s \qquad s \in [s_{break}, s_{end}] \quad (5)$$

The second mode inhibits the first mode [27]. Therefore, the total second mode suction equation can be written as:

$$\mathrm{S}_2(\mathrm{s}) = w_2 \mathrm{S}_{21} + (1 - w_2) S_{22} \qquad s \in [s_{break}, s_{end}] \quad (6)$$

$$w_2 \in [0,1]$$

The final model of the swelling is the addition of S_1 and S_2 in their respective application range:

$$S(s) = S_1(s) + S_2(s) \quad (7)$$

With the following parameters:

S_f: the stabilized swelling percentage at the end of the experiment [%].

C_1: the parameter of the matric swelling function $S_1(s)$ [minutes].

$S_{11}(s)$: the exponential part of the first adsorption mechanism [%].

$S_{12}(s)$: the linear part of the first mode of swelling [%].

C_{11}, C_{12}: the linear parameters of the $S_{12}(s)$equation [minutes].

w_1: the weighting factor of the $S_{11}(s)$ and $S_{12}(s)$ functions to obtain $S_1(s)$ [-].

$\mathrm{S}_{21}(\mathrm{s})$: the exponential part of the second adsorption mechanism [%].

$\mathrm{S}_{22}(\mathrm{s})$: the linear part of the second mechanism [%].

C_{21}, C_{22}: the linear parameters of the $S_{22}(s)$ equation [minutes].

w_2: the weighting factor of the $S_{21}(s)$ and $S_{22}(s)$ functions to obtain $S_2(s)$ [-].

The full theoretical sub-model, $S_1(s)$, is shown in Fig. 6, with the speed and acceleration curves on the y-secondary axis. Table 2 presents the mathematical characteristics of the theoretical model, including the locations of the point of inflection, the primary and secondary swells, and the slope break. Appendix A gives a theoretical formulation of those mathematical characteristics. A synthetic swelling curve with the different swelling curves from Equations 1 to 6 is shown in Fig. 7, where the slope break is evaluated either visually or using the acceleration curve. The procedure for finding the parameters $C_1,\ C_{11},\ C_{12},\ C_{21},\ C_{22}, w_1, w_2$, is given in Appendix B.

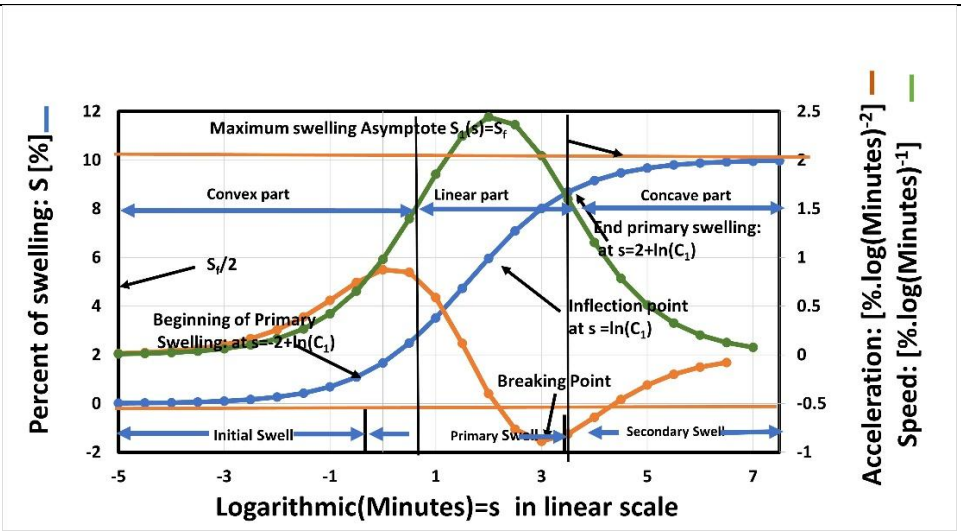


Fig. 6 Example of Theoretical Model: $S(s) = S_f \frac{e^s}{C_1+e^s}$ in "s=log(t) Scale, with Speed and Acceleration in the Secondary Y-Axis $(S_f = 10, C_1 = 5)$

296

Sub-Model	$\boldsymbol{S_1(s) = S_f \frac{e^s}{C_1 + e^s}}$			
	Beginning Primary Swelling	**Inflection Point**	**Theoretical Limits of the Slope Break**	**Ending Primary Swelling**
***s* domain**	$\boldsymbol{\approx -2 + log(C_1)}$	$\boldsymbol{log(C_1)}$	$\boldsymbol{C_1(2+\sqrt{3})}$	$\boldsymbol{\approx 2 + log(C_1)}$
$\boldsymbol{S_1(s)}$	$\boldsymbol{\approx 0.12\, S_f}$	$\boldsymbol{0.5\, S_f}$	$\boldsymbol{0.79\, S_f}$	$\boldsymbol{\approx 0.88\, S_f}$

Table 2 Theoretical Mathematical Singular Points of the Model Equation: $S_1(s) = S_f \frac{e^s}{C_1+e^s}$ (Appendix A)

297

298

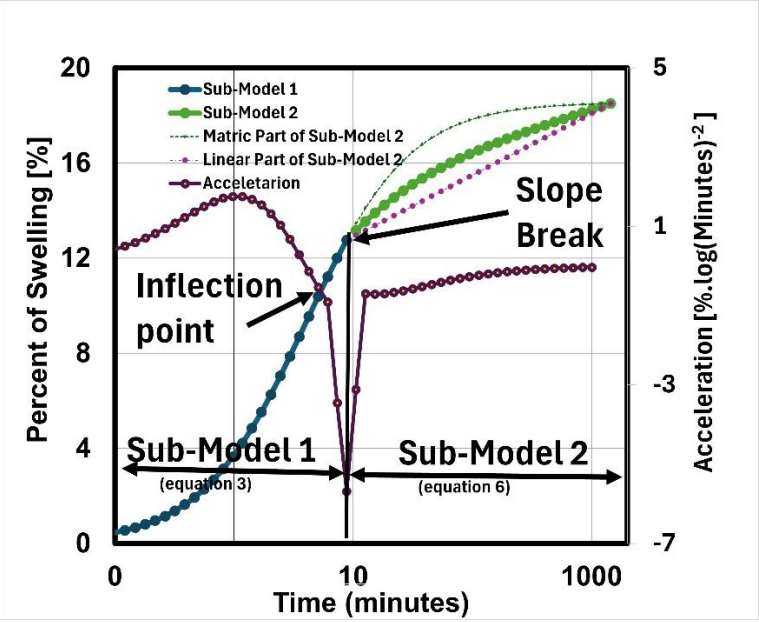


Fig 7 Synthetic Example of Swelling Curves with the Acceleration Curve in the Secondary Axis

299

300

8. Comparison between Swelling Test Results and the New Model

The research aims to evaluate the applicability of the new model (Equations 3 and 6) to describe the swelling behavior of clayey soils exposed to different Sodium and Potassium Chloride solutions. The research involved conducting five test series under fixed vertical pressures. In Figs. 2a and 2b, for the Ariel clay, the constant pressures were 1 kPa and 2 kPa, respectively, using Sodium Chloride Solutions. In Figs. 3a and 3b, at a constant pressure of 1kPa, NaCl and KCl solutions were used for the Ariel clay, respectively. In Figs. 4a and 4b, at a constant pressure of 0.1 kPa, NaCl and KCl solutions were used for the Senneck clay, respectively. For the Ariel Clay, each test series uses solutions with 0%, 5%, 10%, 15%, 20%, and 25% salt weight concentration. For the Senneck-Montmorillonite clay, the test series uses salt concentrations of 0%, 5%, 10%, 15%, and 20%. In Figs 2-4, the new model is plotted alongside the test data, showing a good fit for the five data series. Figures 8a and 8b show two examples of swelling curves for Ariel clay at 10% and 25% Sodium Chloride concentrations, with the acceleration curves plotted on a secondary y-axis. The swelling break slope point is the minimum of the acceleration curve. The location of the inflection point in the test data is determined by the point at which the acceleration curve crosses the zero line. Figures. Figs. 9a and 9b show the final fitted model along with the test data, using the new model explained in section 7 and Appendix B.

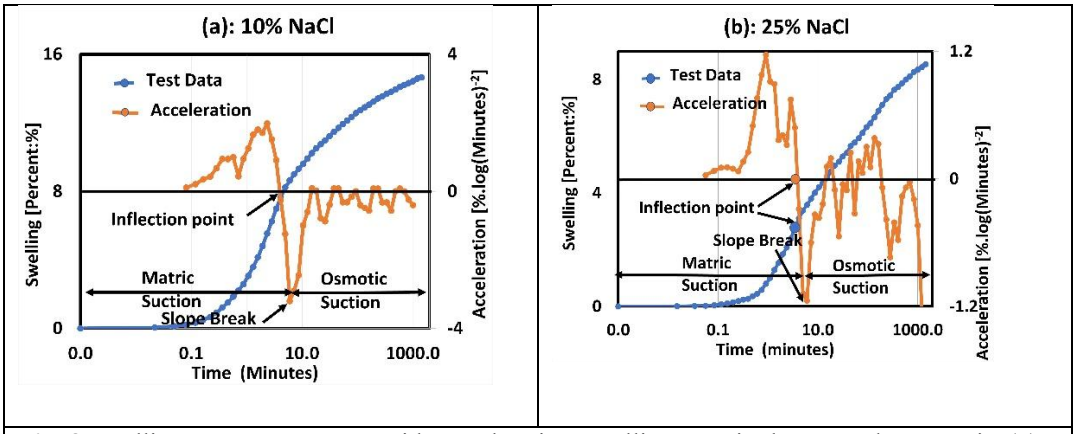


Fig. 8 Swelling Test Data Curves with Acceleration Swelling Rate in the Secondary Y-axis: (**a**) 10% NaCl, (**b**) 25% NaCl, for the Ariel Clay

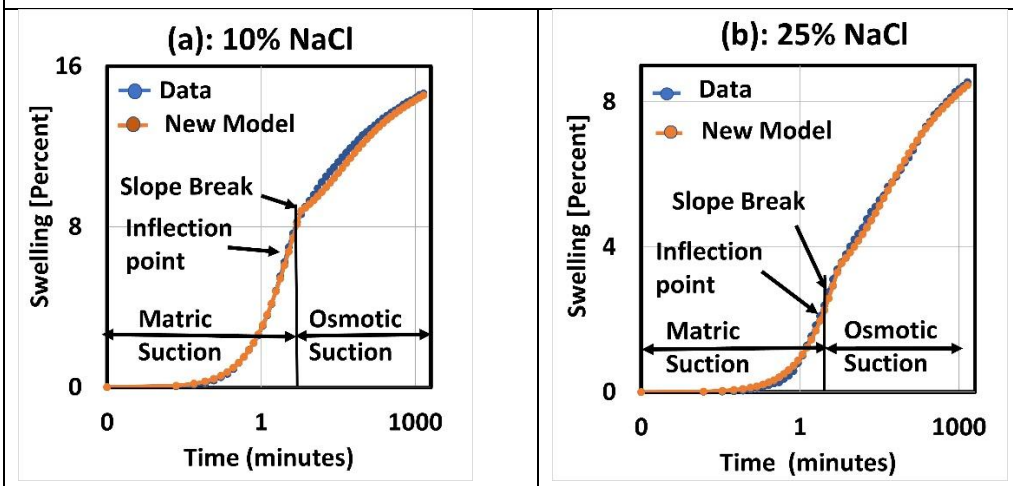


Fig. 9 Swelling Test Data with the New Final Model for the Ariel Clay: **(a)** 10% NaCl, **(b)** 25% NaCl, for the Ariel Clay

320

321

322

Weight Concentration of Sodium Chloride Solution [%]	Ariel Soil, 1kPa NaCl	Ariel Soil, 2kPa NaCl	Ariel Soil, 1kPa KCl	Senneck Soil, 0.1kPa NaCl	Senneck Soil, 0.1kPa KCl
0	0.62 [2.51]	0.32 [2.15]	0.45[1.55]	0.27 [1.25]	0.27[1.49]
5	1.47 [4.81]	0.29 [2.58]	0.57[1.71]	0.25 [1.25]	0.42[0.84]
10	0.60 [3.50]	0.42 [3.50]	0.57[3.74]	0.33 [1.20]	0.44[1.24]
15	0.64 [3.36]	0.40 [2.76]	0.48[1.23]	0.32 [1.63]	0.64[2.29]
20	0.66 [3.35]	0.51 [3.48]	0.77[3.44]	0.27 [1.63]	0.37[2.29]
25	0.87 [4.48]	0.58[3.57]	0.73[5.74]		

Table 3 Normalized RMSE Analysis of the New and Hyperbolic [in brackets] Models for Different Weight Concentrations of Sodium and Potassium Chloride Solutions for the Five Experiments

9. Statistical Analysis

Table 3 compares the Normalised Root Mean Square Error (RMSE) between the test data, the new model, and the PSO hyperbolic model (in brackets) for the five series of experiments. All RMSE values are lower for the new model than for the hyperbolic model, indicating a better fit to the experimental results.

Weight Concentration of Sodium Chloride Solution [%]	Density of Sodium Chloride Solution	Maximum Swelling (After 24 hours) [%]	Ending Moisture [%]	Final Total Unit Weight [kN/m^3]	Final Dry Unit Weight [kN/m^3]	Ending Saturation [%]	Ending Void Ratio [-]	Total Specimen Weight [g.]	Dry Specimen Weight [g.]
0	1	15.65 [10.62]	53.28 [51.36]	17.15 [16.45]	11.19 [11.34]	100 [99.47]	1.50 [1.30]	48.09 [48.85]	31.52 [31.52]
5	1.034	15.15 [10.88]	52.90 [48.94]	16.69 [16.82]	11.04 [11.31]	93.20 [89.5]	1.62 [1.56]	48.05 [46.95]	31.97 [32.03]
10	1.071	10.44 [8.82]	48.48 [47.93]	16.95 [16.58]	11.67 [11.22]	88.31 [81.8]	1.56 [1.67]	48.80 [46.49]	32.53 [32.42]
15	1.108	8.59 [8.06]	47.91 [46.14]	17.19 [16.72]	12.00 [11.44]	86.41 [76.8]	1.58 [1.71]	46.62 [46.07]	32.99 [32.95]
20	1.147	7.33 [4.09]	45.30 [46.58]	17.36 [16.73]	12.44 [11.42]	81.91 [73.1]	1.57 [1.82]	46.66 [47.21]	33.25 [33.41]
25	1.188	8.54 [1.77]	41.11 [47.10]	16.71 [16.31]	12.45 [11.09]	69.49 [67.0]	1.66 [2.00]	44.48 [46.37]	33.57 [33.88]

Table 4 Comparison of Ending Characteristics of the Ariel Clay Samples at Constant Pressure of 1kPa and **2kPa** [**in Bracket**] after 24 Hours Immersion Experiments at Five Different Weight Concentrations of Sodium Chloride

Weight Concentration of Sodium Chloride Solution [%]	Density of Sodium Chloride Solution	Maximum Swelling (After 24 hours) [%]	Ending Moisture [%]	Final Total Unit Weight [kN/m^3]	Final Dry Unit Weight [kN/m^3]	Ending Saturation [%]	Ending Void Ratio [-]	Total Specimen Weight [g.]	Dry Specimen Weight [g.]
0	1 [1]	15.65 [23.88]	53.28 [57.77]	17.15 [16.28]	11.19 [10.32]	100.0 [96.38]	1.50 [1.71]	48.09 [49.74]	31.52 [31.52]
5	1.034 [1.030]	15.15 [14.32]	52.90 [51.55]	16.69 [16.45]	11.04 [11.03]	93.29 [86.79]	1.62 [1.76]	48.05 [47.79]	31.97 [32.49]
10	1.071 [1.063]	10.44 [8.64]	48.48 [50.63]	16.95 [17.28]	11.67 [11.83]	88.31 [84.1]	1.56 [1.72]	48.80 [47.49]	32.53 [33.94]
15	1.108 [1.097]	8.59 [7.24]	47.91 [49.15]	17.19 [16.58]	12.00 [11.54]	86.41 [73.2]	1.58 [1.91]	46.62 [47.02]	32.99 [33.34]
20	1.147 [1.133]	7.33 [14.07]	45.30 [46.18]	17.36 [16.43]	12.44 [11.75]	81.91 [66.1]	1.57 [1.99]	46.66 [46.08]	33.25 [33.66]
25	1.188 [1.172]	8.54 [13.04]	41.11 [43.26]	16.71 [16.57]	12.45 [12.03]	69.49 [64.4]	1.66 [1.91]	4.48 [45.16]	33.57 [33.53]

Table 5 Comparison of Ending Characteristics of the Ariel Clay Samples at Constant Pressure of 1kPa after 24 Hours Immersion Experiments at Five Different Weight Concentrations of Sodium and **Potassium Solutions** [**in Bracket**]

	Density of Sodium Chloride Solution	Maximum Swelling (After 24 hours) [%]	Ending Moisture [%]	Final Total Unit Weight [kN/m^3]	Final Dry Unit Weight [kN/m^3]	Ending Saturation [%]	Ending Void Ratio [-]	Total Specimen Weight [g.]	Dry Specimen Weight [g.]
0	**1**	**45.5 [40.41]**	**106.57 [89.40]**	**15.82 [15.72]**	**7.66 [8.30]**	**100.0 [100.0]**	**2.48 [2.21]**	**37.83 [36.61]**	**19.78 [19.33]**
5	**1.034 [1.030]**	**34.28 [22.38]**	**82.10 [82.14]**	**14.47 [16.22]**	**8.06 [9.03]**	**89.9 [100.00]**	**2.42 [2.05]**	**35.22 [35.75]**	**19.86 [19.88]**
10	**1.071 [1.063]**	**33.71 [17.52]**	**82.63 [75.61]**	**15.29 [16.43]**	**8.63 [9.70]**	**92.54 [100.0]**	**2.27 [1.93]**	**35.75 [35.05]**	**20.64 [20.27]**
15	**1.108[1.097]**	**23.38 [22.76]**	**77.00 [67.60]**	**16.27 [15.73]**	**9.61 [9.73]**	**94.26 [87.59]**	**2.00 [1.91]**	**34.22 [33.36]**	**20.79 [20.56]**
20	**1.147 [1.133]**	**27.15 [20.94]**	**70.44 [62.89]**	**14.48 [15.16]**	**8.93 [9.75]**	**69.7 [72.9]**	**2.75 [2.34]**	**32.93 [32.63]**	**21.07 [20.97]**

Table 6 Comparison of the Ending Characteristics of the Senneck Clay Samples at Constant Pressure of 0.1kPa after 24 hours Immersion Experiments at Four Different Weight Concentrations of Sodium and Potassium [in Bracket] Chloride

10. Geophysical and Microstructural Foundations of Clay Swelling with Salty Water Leading to the New Model

10.1 Computation of the Geotechnical Characteristics

Tables 4, 5, and 6 summarize the geomechanical characteristics of the soil samples after swelling had stabilized at the end of the tests. For Ariel Soil, series No. 1 and No. 2 use Sodium Chloride solutions at 1kPa and 2 kPa, respectively, under constant pressure (Table 4). For Ariel soil, series No. 3 uses Potassium Chloride solutions at a constant pressure of 1kPa (Table 5). For Senneck-Montmorillonite soil, series No. 4 and No. 5 use Sodium and Potassium Chloride solutions, respectively, at a constant pressure of 0.1 kPa (Table 6). As the concentration of salt increases, the following conclusions can be drawn:

- The maximum swelling, the final moisture content, the final saturation, and the final total specimen weight decrease due to a decrease in water adsorption.
- The void ratio tends to increase for the Ariel clay soil. In contrast, for the Senneck-clay soil, the void ratio decreases until *the minimum possible swelling* percentage is reached at a specific salt concentration, then increases.
- The dry weight and the dry unit weight of the specimen increase with the addition of salt.

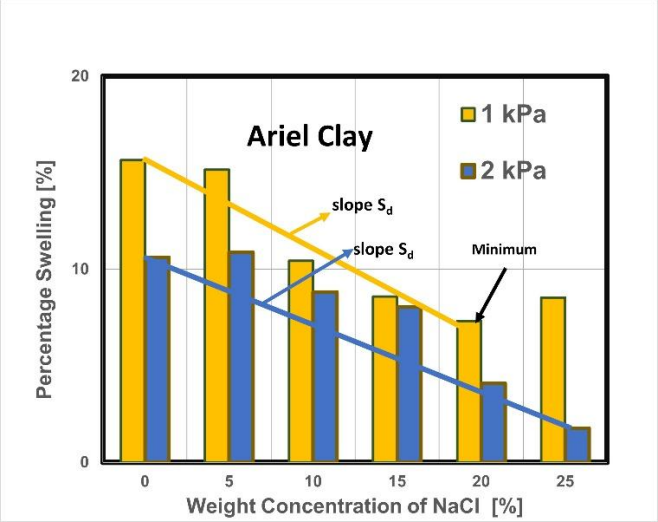


Fig. 10 Comparison of Maximum Percentage Swelling versus Weight Concentration of Sodium Chloride Solutions at 1kPa and 2kPa Constant Pressure Conditions for the Ariel Clay

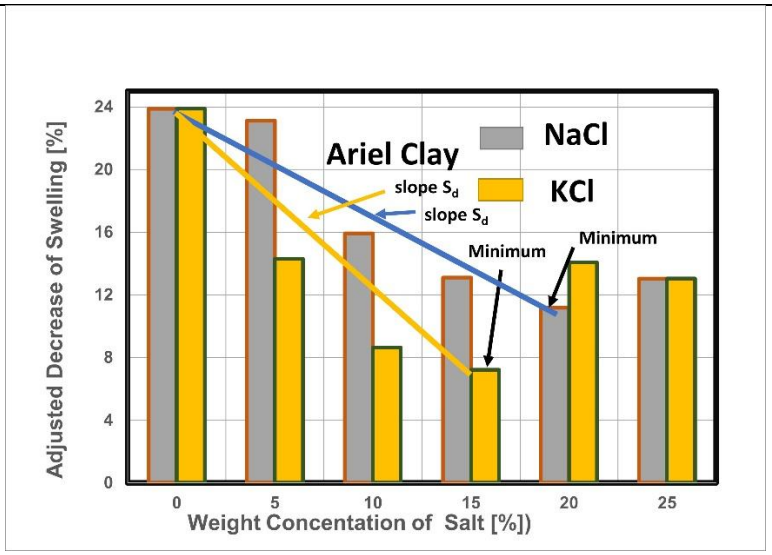


Fig. 11 Comparison of Maximum Percentage of Swelling versus Weight Concentration of Sodium and Potassium Chloride at 1kPa Constant Pressure Condition for the Ariel Clay

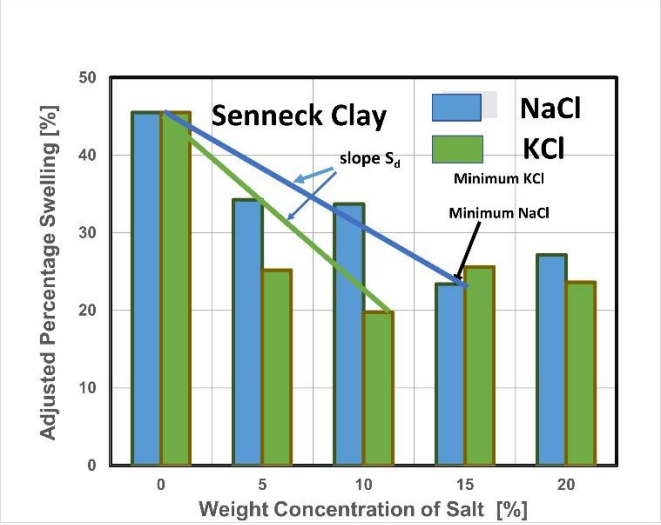


Fig. 12 Comparison of Maximum Percentage of Swelling versus Weight Concentration of Sodium and Potassium Chloride Solutions at 0.1kPa Constant Pressure Condition for the Senneck-Montmorillonite Clay

Type of Soil	**Ariel Soil**		**Ariel Soil (Adjusted)**		**Senneck Soil**	
Constant Pressure [kPa]	**1**	**2**	**1**	**1**	**0.1**	**0.1**
Type Solution	**NaCl**		**NaCl**	**KCl**	**NaCl**	**KCl**
Adjusted Parameter S_d	**1.23**	**1.50**	**1.23**	**2.10**	**1.5**	**2.94**
Salt weight Concentration at Maximum Swelling Decrease [%]	**20**	**25**	**20**	**15**	**15**	**10**

Table 7 Summary of Efficiency in Decreasing Swelling as a Function of Salt Weight Concentration for the Five Series Experiments

10.2 Comparison of the Swelling Decrease Rate Between the Different Experiment Series

Figures 10-12 illustrate the decrease of swelling as a function of salt concentration and compare them by applied pressure and electrolyte type. A new "*linear swelling decrease rate per weight salt concentration*" parameter is defined as follows:

$$S_d = \frac{S_{0\%} - S_{min\%}}{C_{*\%}} \qquad [\%.l/g.] \qquad (8)$$

$S_{0\%}$: the maximum swelling values for distilled water [%],

$S_{min\%}$: the minimum possible swelling value, [%],

$C_{*\%}$: the weight salt concentration when the minimum swelling occurs $[^{g.}/_{l.}]$.

The parameter S_d is expressed in percentage per salt weight concentration. It must be adjusted to compare across experiments; the larger the parameter, the greater the reduction in swelling. The following conclusions can be derived from the Figs. 10-12 and Table 7:

- The decrease in swelling is more efficient at low pressure.
- Potassium chloride solutions are more effective at reducing swelling than Sodium chloride solutions. The difference in ionic radius between K^+ and Na^+ cations explained the difference in swelling ([32].
- The swelling percentage reaches *a minimum at a specific salt concentration*, then increases slightly at higher concentrations. Osmotic swelling is caused by the concentration difference between ions held electrostatically at the clay layers and those in the pore water of the clay soil. An increase in the number of cations in the pore water results in an expansion of the clay's interlayer spacing in the DDL. The minimum swelling can be explained by the amount of saline water required to establish electrical equilibrium between the interlayer clay and the pore water in the clay soil. However, there is a maximum possible concentration value of cations in the inter-clay layer. The concentration in the clay inter-sheet layer remains stable while the concentration of cations in pore water continues to increase; therefore, the osmotic swelling slightly intensifies after reaching a minimum [23].

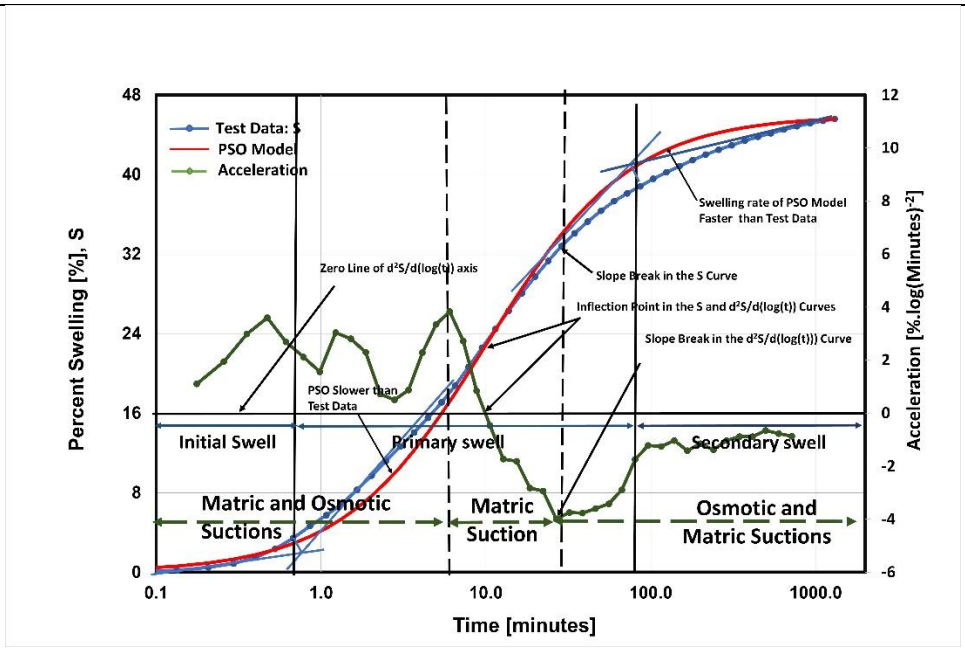


Fig. 13 Senneck-Montmorillonite Clay Swelling in the Primary Y-Axis and Acceleration Rate Curve in the Secondary Y-Axis

10.3 Swelling of Montmorillonite Clays Using Pure Water and Potassium Chloride Solutions.

Figures 4 and 13 illustrate swelling in Montmorillonite clay. The following conclusions can be drawn:

10.3.1 Swelling of Montmorillonite Clay using Distilled Water.

A pronounced swelling phenomenon occurs in clayey soils, such as Montmorillonite, which have weak ionic interlayer bonding, when immersed in distilled water, as shown in Fig. 13. The swelling curve exhibits an S-shape, comprising three distinct rate regions: initial, primary, and secondary swelling. Their limits are defined by the intersections of the tangents to the three main slopes of the swelling curve: initial, primary, and secondary. Figure 13 also displays the acceleration, $\left(\frac{d^2S}{d(log(t))}\right)$, of the experimental swelling data on the secondary y-axis. The intersection of the acceleration curve with the zero acceleration y-axis line indicates the location of the inflection point in the s=log(t) domain. The minimum acceleration value provides *the exact time of the breaking point*, at which the osmotic mechanism of absorption becomes more perceptible. In the swelling phenomenon of Montmorillonite-clay soils containing distilled water, the matric swelling is *predominant*, while diffuse double-layer swelling is *less important but still exists*. The inflection point occurs at an amplitude of almost half of the swelling. However, an acceleration of adsorption is observed before the inflection point, and a slowing of adsorption is observed after the inflection point compared to a standard Pseudo-Secondary Order (PSO) model. That suggests that two simultaneous adsorption processes occurred. Osmotic suction accelerates at the beginning and inhibits at the end of the swelling process.[27]. The strong water adsorption may be explained by the very weak interlayer bonds in the clay. The distance between the clay sheets is large, attracting many water molecules to the negatively polarised clay surface [35], making the first (matric) part of the adsorption relatively strong and rapid. The second part of adsorption (osmotic swelling) is weaker than the first (matric swelling) because there are fewer free cations in the solutions, allowing them to enter the inter-sheet space. Figure 13 illustrates that the separation between preponderant matric and preponderant osmotic suction is defined by the slope break, also expressed by a strong minimum in the acceleration curve. This separation is not the same at the same location as the separation between primary and secondary swell.

10.3.2 Swelling of Ca-Montmorillonite using Sodium and Potassium Chloride Solutions.

Figures. 4a and 4b show the test results obtained for Senneck-Montmorillonite clay with varying percentages of Sodium and Potassium Chloride. The S-shape of the curve stays longer in Montmorillonite than in Illite (Figure 3). The percentage of the first adsorption mode is greater than

that in Illite clays (Figures 3-4 and Tables 8-10). According to these results, the predominant first (matric) part of the adsorption process is more pronounced in Potassium Chloride solutions than in Sodium Chloride solutions until a salt weight concentration of 10%. For concentrations above 10%, the first mode is more pronounced in NaCl solutions. However, Potassium Chloride solutions are more effective at reducing swelling. That means the main contribution to the decrease in swelling occurs during the first mode. The strong first adsorption mechanism at the initial stage of the swelling process is more inhibited using Potassium Chloride solutions than Sodium Chloride solutions. The cations Na^+ or K^+ in Sodium or Potassium Chloride solutions may enter the structure of Ca-montmorillonite through cation exchange between Ca^{++} in the clay sheet and Na^+ or K^+ in the solution, thereby decreasing the second phase of swelling [32]. The cation exchange is greater for K^+ than Na^+ cations, making the osmotic swelling relatively weaker for Potassium Chloride solutions than the Sodium Chloride solutions [31]

	Pression	Parameters	0%	5%	10%	15%	20%	25%	Row
Ariel Clay, NaCl	1 kPa	Maximum Swelling S_f [%]	15.65	15.15	10.44	8.62	7.33	8.54	1
	2 kPa		10.62	10.88	8.82	8.06	4.09	1.77	
	1 kPa	Parameter C_1	3.76	3.85	7.28	4.33	8.84	7.29	2
	2 kPa		5.34	3.40	4.41	4.29	23.32	90.94	
	1 kPa	Swelling at Breaking Point S_b [%]	6.82	7.19	4.21	2.65	3.60	3.11	3
	2 kPa		5.35	5.50	4.18	3.16	2.67	0.98	
	1 kPa	Time at Breaking Point t_b [min.]	2.90	3.48	4.91	1.65	8.54	4.18	4
	2 kPa		3.48	3.48	3.98	2.76	65.12	112.83	
	1 kPa	Max. Speed of the Swelling Curve [%/log(min.)]	4.60	4.20	2.20	1.65	1.30	1.80	5
	2 kPa		2.61	2.89	2.41	1.93	0.71	0.45	
	1 kPa	Time at the Inflection Point t_i [min.]	2.00	1.99	3.35	0.89	1.43	3.47	6
	2 kPa		1.65	2.40	2.19	1.86	45.11	93.96	
	1 kPa	Relative Percentage of First mode [%]	43.56	43.51	40.30	30.70	49.16	36.45	7
	2 kPa		50.38	50.56	43.65	39.17	48.07	55.37	
	1 kPa	Slope of the Second Part [%/log(min.)]	1.42	1.32	1.10	0.89	0.73	0.93	8
	2 kPa		0.84	0.89	0.79	0.78	0.51	0.31	
	1 kPa	Percent of Osmose in the Second Mode [%]	50	50	80	70	80	80	9
	2 kPa		50	50	65	60	80	95	

Table 8 Geo-Mathematical Characteristics of the Swelling Curves from the Two Series of Experiments Comparing the Effect of Sodium Chloride Solutions for the Ariel Clay at 1 kPa and 2 kPa Constant Pressure**.**

	Solutions	*Parameters*	0%	5%	10%	15%	20%	25%	Row
Ariel Clay, 1kPa	NaCl	Maximum Swelling S_f [%]	15.65	15.15	10.44	8.62	7.33	8.54	1
	KCl		23.45	18.57	14.77	13.52	13.93	15.41	
	NaCl	Parameter C_1	3.76	3.85	7.28	4.33	8.84	7.29	2
	KCl		5.34	3.64	3.45	5.42	5.24	4.45	
	NaCl	Swelling at Breaking Point S_b [%]	6.82	7.19	4.21	2.65	3.60	3.11	3
	KCl		13.15	9.99	6.73	7.76	4.96	4.68	
	NaCl	Time at Breaking Point t_b [min.]	2.90	3.48	4.91	1.65	8.54	4.18	4
	KCl		7.32	4.24	2.89	7.30	2.90	1.94	
	NaCl	Max. Speed of the Swelling Curve [%/log(min.)]	4.60	4.20	2.20	1.65	1.30	1.80	5
	KCl		5.92	4.55	3.28	3.78	2.59	3.54	
	NaCl	Time at the Inflection Point t_i [min.]	2.00	1.99	3.35	0.89	1.43	3.47	6
	KCl		4.23	2.94	1.65	5.05	1.13	1.31	
	NaCl	Relative Percentage of First mode to the Maximum Swelling [%]	43.56	43.51	40.30	30.70	49.16	36.43	7
	KCl		56.08	53.79	45.58	57.35	35.63	41.24	
	NaCl	Slope of the Second Part [%/log(min.)]	1.42	1.32	1.10	0.89	0.73	0.93	8
	KCl		1.95	1.47	1.29	1.09	1.44	1.62	
	NaCl	Percent of Osmose in the Second Mode [%]	50	50	80	70	80	80	9
	KCl		40	50	70	80	100	95	

Table 9 Geo-Mathematical Characteristics of the Swelling Curves from the Two Series of Experiments Comparing the Effect of Sodium and Potassium Chloride Solutions for the Ariel Clay at 1 kPa for Sodium and Potassium Chloride Solutions

	Solutions	Parameters	0%	5%	10%	15%	20%	Row
Senneck 0.1kPa	NaCl	Maximum Swelling S_f [%]	45.66	34.28	33.71	23.38	27.15	1
	KCl		40.41	22.38	17.53	22.76	20.94	
	NaCl	Parameter C_1	11.42	7.80	16.19	25.05	11.41	2
	KCl		8.74	5.59	9.98	7.32	8.00	
	NaCl	Swelling at Breaking Point S_b [%]	33.48	25.84	22.19	18.80	19.63	3
	KCl		31.03	18.15	15.03	15.79	14.89	
	NaCl	Time at Breaking Point t_b [min.]	31.37	23.86	31.20	102.87	29.75	4
	KCl		28.90	23.97	59.92	16.61	19.66	
	NaCl	Max. Speed of the Swelling Curve [%/log(min.)]	10.11	7.71	7.53	4.33	5.06	5
	KCl		9.59	6.26	3.81	5.83	5.59	
	NaCl	Time at the Inflection Point t_i [min.]	8.59	11.32	14.84	12.71	7.75	6
	KCl		13.85	13.76	23.86	11.47	11.16	
	NaCl	Relative Percentage of First Mode to the Maximum Swelling [%]	73.31	75.37	72.65	80.42	72.28	7
	KCl		73.57	81.65	85.72	72.69	67.78	
	NaCl	Slope of the Second Part [%/log(min.)]	3.03	1.93	2.55	1.74	1.60	8
	KCl		2.23	1.03	0.71	1.27	1.33	
	NaCl	Percent of Osmose in the Second Mode [%]	50	40	65	60	60	9
	KCl		40	0	60	90	90	

Table 10 Geo-Mathematical Characteristics of the Swelling Curves from the Two Series of Experiments Comparing the Effect of Salty Solutions for the Senneck Clay at 0.1 kPa for Sodium and Potassium Chloride Solutions

10.4 Interpretation of Parameters of the New Swelling Model: C_1, C_{22} and, w

The swelling phenomenon is due to the presence of free, dipolar-polarized water molecules in the solution in contact with clay minerals. Dipolar water molecules attracted to the clay inter-sheet space cause clay swelling in two modes: attraction to the polarized clay sheet surface, resulting in several organized water layers, and attraction to free cations away from the clay surface, forming ion-water clusters. The dissolution of salt in water induces a diminution of free dipolar water molecules and an increase in the concentration of free cations in the solution. This change in water chemistry may lead to reduced swelling in both modes: fewer water layers for the first mode of adsorption and fewer cation-water clusters in DDL for the second mode, resulting in a decrease in the stabilized swelling maximum and a decrease in the swelling rate. From Tables 8-10, in absolute value, the diminution in function of salt weight concentration is more rapid for the first mode of adsorption than for the second mode . The first mode predominates at the beginning of the swelling for a short time, and the second mode predominates thereafter for a longer time until the swelling stabilizes. The two modes may occur simultaneously, influencing each other during the swelling process. The two preponderant modes are separated by a visible slope break in the swelling curve or a strong minimum in the acceleration curve, both expressed in the s-domain. To model the swelling curve shape, it is sufficient to know the position of the breaking point and the position at the end of the stabilized experiment, both in logarithm of time and amplitude, as explained in Appendix B. Tables 8-10 present some geo-mathematical parameters observed or computed from all the experiment swelling curves presented in Figs .2-4**,** using all swelling, speed and acceleration curves (as in Figure 5): 1 the maximum swelling, 2) the parameter. C_1 of the swelling curve, 3) the position of the slope break, 4) the position of the inflection point, 5) the slope of the linear part of the second mode of adsorption, 6) the relative percentage of the preponderant first mode of adsorption, 7) the relative percentage of linearity (osmose) in the second preponderant mode.

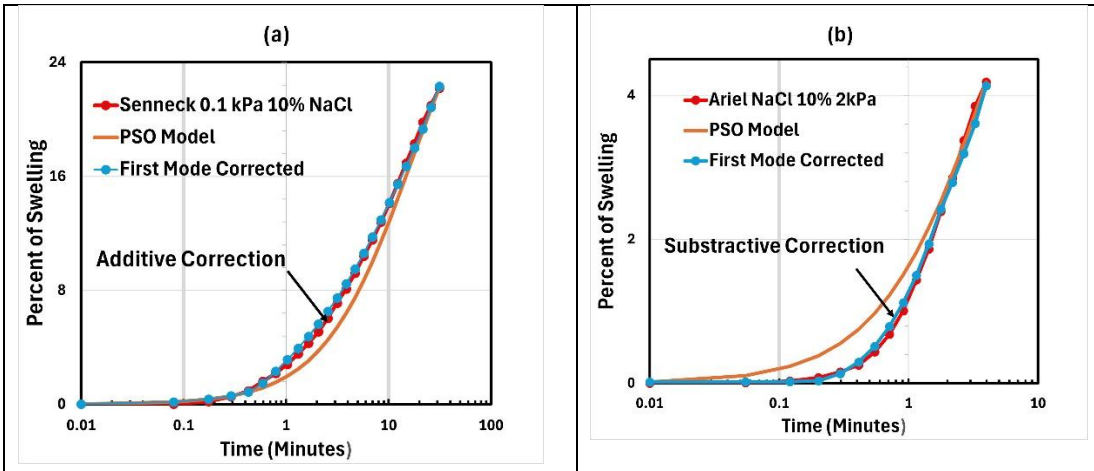


Fig 14: Examples of (**a**) Subtractive and (**b**) Additive Corrections of the First mode of Adsorption due to the Second mode of Adsorption

10.4.1 Parameters of the First Mode of Adsorption

The only parameter that describes the shape and the rate of the first part of the swelling curve is C_1, as described in Equation (1). A small value C_1 makes adsorption rapid, whereas a larger value slows it. The theoretical S-shape of swelling in the *s*-domain is depicted by a concave shape at the beginning and a convex shape at the end of the swelling process. The bigger the parameter C_1, the larger the S-Shape along the *s*-axis, making the concave part less concave and the convex part less convex. A very high value C_1 makes the adsorption quasi-linear in the s-domain. For example, for the distilled water experiment, the value C_1 is at least three times bigger for Montmorillonite Clay than for Illite Clay (Tables 9-10). However, the maximum swelling is greater for Montmorillonite than for Illite (Figures 2-a and 4-a, and Tables 8 and 10**).** The parameter C_1 tends to increase with increasing salt concentration, making the S-shape larger in the s-domain and thus more linear (Figures 2-4).

The parameter C_1 depends on the type of clay, the constant pressure applied to the clay specimen, and the salt concentration in the solution. It is independent of the maximum swelling. The maximum swelling amplitude depends on the type of clay, the constant pressure applied to the clay specimen, the solution's salt concentration, the soil's density, and its Atterberg limits. It requires another model to describe it [1-4].

Because the two modes of adsorption may occur simultaneously, the second mode may influence the first mode, either by inhibition (Illite) or by acceleration (Montmorillonite), beyond the calculated swelling-rate parameter C_1. Sometimes, there is no effect on the first adsorption mode.

The proposed model accounts for potential inhibition or acceleration as described in Equation (2).

When using Montmorillonite clay, the first adsorption mode is accelerated in both NaCl and KCl solutions, as shown in Fig. 14a .The shape of the curve becomes less concave. The acceleration observed when using Montmorillonite clay can be explained by the weak inter-sheet bonds in Montmorillonite, which make the matric part of adsorption stronger and easier. The osmotic component of the swelling does not inhibit the first mode; rather, it accelerates it. The electrostatic forces attracting the dipolar water molecules at the surface of the clay sheet are stronger than the electrostatic forces attracting the dipolar water molecules to free ions in the inter-sheet space[27].

When using Illite and NaCl solutions, the first adsorption mode is inhibited, as shown in Fig. 14-b. The curve is becoming more concave, indicating a slowing of adsorption of the first mode. This can be explained by the fact that stronger inter-sheet bonds weaken matric adsorption, thereby inhibiting the adsorption of organized water layers by osmotic adsorption.

When using Illite with KCl solutions, no inhibition or acceleration is observed in the first adsorption mode. The two modes of adsorption do not interfere with each other during the initial stage.

10.4.2 Parameters of the Second Mode of Adsorption

The model parameters of the second adsorption mode are $(C_1, C_{12}, C_{22}$, and $w_2)$ in Equations 4-6. C_{22} is the slope of a straight line describing a pure second-mode adsorption and C_{12} is its intercept on the y-axis. The parameter w_2 represents the linearity component in the second adsorption mode. The larger this parameter is, the more linear the second part of the adsorption curve is. Equation 1 is the expression of the pure first mode of adsorption, which is supposed to be sigmoid in the s-domain. Equation 5 represents the straight line, expression of the pure second mode of swelling after the breaking point. This straight line passes through the breaking point and goes to the end point of the experiment. The influence of the osmotic adsorption mode is more pronounced in the second mode than in the first. That is why a break point is visible in the s-domain swelling curve. The second part of adsorption is a weighted average of hyperbolic and logarithmic adsorption shapes in the time domain or sigmoid and linear shapes in the s-domain. In the acceleration graph, after the breaking point, the more frequent the succession of maxima and minima, the more linear the second part of adsorption. As the salt concentration increases, the number of minima and maxima increases. This indicates a non-continuous, cascaded type adsorption process. This cascade of acceleration and deceleration demonstrates the linearity, slowness, and weakness of the second adsorption mode. The strong attraction of water molecules to free cations accelerates, and after forming clusters with water molecules, a release occurs, causing an electrochemical imbalance that is then filled by a new attraction to dipolar water molecules.

10.4.3 Influence of Salty Solutions on the Shape of the Absorption Curves.

Tables 8-10 show the influence of salty solutions on the geometric characteristics of the swelling

curves as a function of salt concentration. The following conclusions can be drawn as the salt concentration increases:

- The maximum amplitude decreases (row 1 of Tables 8-10)
- The "C_1" value increases, making the first part of the curve larger and slower (row 2 of Tables 8-10),
- The breaking point occurs earlier and at a lower percentage of swelling (rows 3 and 4 of Tables 8-10),
- The maximum speed (defined by the maximum of the first derivative curve) decreases (row 5 of Tables 8-10),
- The inflection point occurs earlier at a lower percentage of swelling (row 6).
- The *relative* part of the first mode of adsorption decreases, while the relative part of the second mode of adsorption increases (row 7 of Tables 8-10),
- The linearity part of the adsorption increases in the second mode (parameter w) increases, slowing the second part of the adsorption (row 9 of Tables 8-10).
- It is interesting to note that using Montmorillonite clay, the shape of the first part of the swelling is the same, i.e., the parameter C_1 stays stable, and the percentage of matric adsorption also remains stable, indicating a strong first adsorption.

11. Conclusions

- The new suggested model represents the behavior of the swelling clayey soils observed in the laboratory relatively well, and there is a reasonable agreement between the model analysis and the test results presented in this research work.
- The amount of swelling was represented as a function of the logarithm of time (s), the variable for which the model was developed. On the logarithmic scale of time, the two mechanisms of swelling — which may be identified as innercrystalline and DDL osmotic — are easily observed and modeled with relative accuracy.
- Two different equations defined the two mechanisms.
- The test results show that the two mechanisms occurred simultaneously, with a preponderance of matric swelling at the beginning for a shorter time, followed by a preponderance of osmotic swelling at the end for a longer time.
- The limit between preponderant matric suction and preponderant osmotic suction can be defined at the minimum of the acceleration curve in the *s* variable.
- In Montmorillonite soil, using distilled water, the two swelling phases are less easily observed due to the preponderance of matric suction in the swelling curve. They are more easily seen in the acceleration curves. However, they are modeled with reasonable accuracy.
- According to the test results, the swelling percentage decreases when the weight concentration of Sodium or Potassium Chloride increases.

- The test results show that the swelling decreases when the constant load increases.
- The maximum swelling, the final moisture content, the final saturation, and the final total specimen weight decrease as the weight concentration of salt increases in the solution.
- For each tested clay soil, there is a maximum level of Sodium and Potassium chloride adsorption, which means that beyond this level, adding Sodium or Potassium chloride to the solution is ineffective in reducing swelling.
- According to the test results, Potassium Chloride is more efficient in decreasing swelling than Sodium Chloride due to the difference in atomic radius between Na+ and K+ in these solutions, respectively.

11. Authors' Contributions

All the authors contributed to the study conception and design. David Benoliel performed material preparation, data collection, and analysis. David Benoliel wrote the first draft of the manuscript, and all the authors commented on earlier versions. All authors read and approved the final manuscript.

12. Funding

The authors did not receive support from any organization for the submitted work. The authors declare no financial interest.

13. Data availability

The Data that support the findings of this study are available from the corresponding author, D.S. Benoliel, e-mail: Davidbo@ariel.ac.il.

14. Competing Interest Information

The authors have no financial or proprietary interests in any material discussed in this article.

References

[1] Nayak N, Christensen R (1971) Swelling Characteristics of Compacted Expansive Soils. Clays and Clay Minerals 19: 251–261, https://doi.org/10.1346/CCMN.1971.0190406

[2] David D, Komornik A, Goldberg M (1973) Swelling and Bearing Characteristics in Clayey Sands and Loess. In Proceedings of the Eighth International Conference on Soil Mechanics and Foundation Engineering, Moscow: 61-65

[3] Mowafy YM, Bauer GE (1985) Prediction of Swelling Pressure and Factors Affecting the Swell Behaviour of an Expansive Soil. Transportation Research Record 1032: 23-28

123 **[4]** Djedid A, Ouadah N (2013) Indirect Estimation of Swelling Clay Soils Parameters. EDGE 18,
124 https://doi.org/10.1080/10916466.2021.2007125

125 **[5]** Dakshanamurthy V (1978) A New Method to Predict Swelling Using a Hyperbolic Equation.
126 Geotechnical Engineering, 9(1): 29-38

127 **[6]** Parcevaux P (1980) Étude Microscopique et Macroscopique du Gonflement des Sols Argileux.
128 Dissertation, Université Pierre et Marie Curie, Paris.

129 **[7]** Vayssade B (1978) Contribution à l'Etude du Gonflement Interparticulaire des Sols Argileux.
130 Dissertation, Ecole Nationale Supérieure des Mines de Paris

131 [8] Al-Mukhtar M, Touray JC, Bergaya F (1999) Une argile modèle pour l'étude du gonflement
132 des sols argileux : la laponite-Na de synthèse. Comptes Rendus de l'Académie des Sciences-Series,
133 Earth and Planetary Science, 329(4) : 239-242.,https://doi.org/10.1016/S1251-8050(99)80241-9

134 **[9]** Al-Mhaidib AI (2008) Mathematical model to predict swelling of expansive soil. In The 12th
135 International Conference of International Association for Computer Methods and Advances in
136 Geomechanics, (IACMAG) 1-6 October, Goa India.

137 **[10]** Sridharan A, Gurtug Y (2004) Swelling behaviour of compacted fine-grained
138 soils. Engineering geology, 72(1-2): 9–18, https://doi.org/10.1016/S0013-7952(03)00161-3

139 **[11]** Komornik U, Benoliel D (2024) A New Model for Evaluating the Behaviour of Swelling
140 Soils. International Journal of Geosynthetics and Ground Engineering 10:79,
141 https://doi.org/10.1007/s40891-024-00580-0

142 **[12]** Lalji SM, Ali SI, Awan ZUH, Jawed Y (2021) A novel Technique for the Modelling of Shale
143 Swelling Behaviour in Water-based drilling Fluids. Journal of Petroleum Exploration and
144 Production Technology 11:3421-3435, https://doi.org/10.1007/s13202-021-01236-9.

145 **[13]** He Y, Ye WM, Chen YG et al (2020) Effects of NaCl solution on the swelling and shrinkage
146 behavior of compacted bentonite under one-dimensional conditions. Bulletin of Engineering
147 Geology and the Environment 79: 399-410, https://doi.org/10.1007/s10064-019-01568-1

148 **[14]** Rao SM, Thyagaraj T, Thomas HR (2006). Swelling of compacted clay under osmotic
149 gradients. Géotechnique, 56(10): 707-713.

150 **[15]** Ahmed AA, Saaid IM, Akhir NAM, Rashedi M (2016) Influence of various cation valence,
151 salinity, pH, and temperature on bentonite swelling behaviour. In AIP Conference
152 Proceedings (Vol. 1774, No. 1). AIP Publishing.,, https://doi.org/10.1063/1.4965087

153 **[16]** Reddy NG, Tahasildar J, Rao BH (2015) Evaluating the influence of additives on swelling
154 characteristics of expansive soils. International Journal of Geosynthetics and Ground
155 Engineering, 1: 1–13

156 **[17]** Biglari M, Yasrobi SS (2005) Effects of NaCl solution on free swelling behavior of
157 compacted clays. In Proceedings of International Conference on Problematic Soils: 25-27

158 **[18]** Hachichi A, Bourokba S, Fleureau JM (2007) Stabilisation chimique de deux sols gonflants
159 de la région d'Oran. Revue française de géotechnique, 118: 3-11,
160 https://doi.org/10.1051/geotech/2007118003

161 **[19]** Belabbaci Z, Mamoune SMA, Bekkouche A (2013) Laboratory Study of the Influence of
162 Mineral Salts on Swelling (KCl, MgCl2). Earth Science Research, 2(2), 135-142, DOI:
163 10.5539/esr.v2n2p135

164 **[20]** Shukla RP, Parihar NS, Gupta AK (2018) Stabilization of expansive soil using potassium
165 chloride. Stavební Obzor – Civil Engineering Journal, 27(1),
166 https://doi.org/10.14311/CEJ.2018.01.0003

167 **[21]** Zumrawi MM, Mahjoub AM, Alnour IM (2016) Effect of some chloride salts on swelling
168 properties of expansive soil. University Of Khartoum Engineering Journal, 6(2): 35-41

169 **[22]** Ladd CC (1960) Mechanisms of swelling by compacted clay. Highway Research Board
170 Bulletin, 245: 10–26, http://onlinepubs.trb.org/Onlinepubs/hrbbulletin/245/245-002.pd

171 **[23]** Madsen FT, Müller-Vonmoos M (1989) The swelling behaviour of clays. Applied Clay
172 Science, 4(2): 143-156, https://doi.org/10.1016/0169-1317(89)90005-7

173 **[24]** Hensen EJ, Smit B (2002) Why clays swell. The Journal of Physical Chemistry B 106: 12664-
174 12667, https://doi.org/10.1021/jp0264883

175 **[25]** Kumari N, Mohan C (2021) Basics of clay minerals and their characteristic properties. Clay
176 Clay Miner, 24(1)

177 [26] Sivapullaiah PV, Hari Prasad Reddy P (2010) Potassium chloride treatment to control alkali-
178 induced heave in black cotton soil. Geotechnical and Geological Engineering 28: 27-36,
179 https://doi.org/10.1007/s10706-009-9274-z

180 **[27]** Thyagaraj T, Salini U (2015) Effect of pore fluid osmotic suction on matric and total suctions
181 of compacted clay. Géotechnique 65(11): 952-960, https://doi.org/10.1680/jgeot.14.P.210

182 **[28]** Rao SM, Thyagaraj T, Raghuveer Rao P (2013) Crystalline and osmotic swelling of an
183 expansive clay inundated with sodium chloride solutions. Geotechnical and Geological
184 Engineering, 31:1399-1404,

185 **[29]** Al-Omari R, Ibrahim SF, Al-Bayati IK (2010) Effect of potassium chloride on cyclic
186 behavior of expansive clays. International Journal of Geotechnical Engineering 4(2): 231-239,
187 DOI: 10.3328/IJGE.2010.04.02.231-239

[30] He Y, Ye WM, Chen YG, Cui YJ (2019) Effects of K+ solutions on swelling behavior of compacted GMZ bentonite. Engineering Geology 249: 241-248, https://doi.org/10.1016/j.enggeo.2018.12.020

[31] Yilmaz I, Marschalko M (2014) The effect of different types of water on the swelling behaviour of expansive clays. Bulletin of Engineering Geology and the Environment, 73: 1049-1062, https://doi.org/10.1007/s10064-014-0598-4

[32] Di Maio C (1996). Exposure of bentonite to salt solution: osmotic and mechanical effects. Géotechnique, 46(4): 695-707, https://doi.org/10.1680/geot.1996.46.4.695

[33] Ye WM, Zhang F, Chen B, Chen, YG, Wang Q et al, (2014) Effects of salt solutions on the hydro-mechanical behavior of compacted GMZ01 Bentonite. Environmental Earth Sciences, 72: 2621-2630.

[34] Ye WM, Zhu CM, Chen YG et al (2015) Influence of salt solutions on the swelling behavior of the compacted GMZ01 bentonite. Environ Earth Sci 74: 793–802, DOI 10.1007/s12665-015-4108-1

[35] Das B (2012) Principles of Geotechnical Engineering,7th Edn.Cengage Learning

[36] ASTM D4546-08 (2008) Standard-Based Model for Swell Characterisation of Expansive Clays. ASTM International, West Conshohocken, PA, USA.

[37] ASTM D4318-17 (2017) Liquid Limit, Plastic Limit, and Plasticity Index of Soils. ASTM International, West Conshohocken, PA, USA.

Appendix A:

Mathematical Properties of the Model of Equation 1 (Table 2)

A.1: How to Find the Inflection Point of the Curve $S(s) = S_f \frac{e^s}{C_1+e^s}$

Starting with the equation:

$$S(s) = S_f \frac{e^s}{C_1+e^s} \qquad \text{A.1}$$

Taking the second derivative

$$S''(s) = \frac{S_f C_1 (e^s - C_1)}{(C_1 + e^s)^3} \qquad \text{A.2}$$

The inflection occurs when $S''(s) = 0$

$$s = log(C_1) \qquad \text{A.3}$$

$$S\big(log(C_1)\big) = \frac{S_f}{2} \qquad \text{A.4}$$

A.2 How to Find the Approximate Limits between the Initial, Primary, and Secondary Phases of Swelling of the Equation $S(s) = \frac{S_f e^s}{C_1 + e^s}$

Equation of the tangent line $Z_{(s=log(C_1))}(s)$, at the inflection point of the function $S(s) = \frac{S_f e^s}{C_1 + e^s}$:

$$Z_{(s=\log(C_1))}(s) = \frac{S_f}{4}(2 - log(C_1) + s) \qquad \text{A.6}$$

Equation of the tangent line $Z_{(s=s_i)}(s)$, at any point $s = s_i$ of the function $S(s) = \frac{S_f e^s}{C_1 + e^s}$:

$$Z_{(s=s_i)}(s) = \frac{S_f e^{s_i}}{C_1 + e^{s_i}}\left(1 + \frac{C_1}{C_1 + e^{s_i}}(s - s_i)\right) \qquad \text{A.7}$$

The intersection of any tangent with the tangent at the inflection point is:

$$Z_{s=\log(C_1)}\,(s) = Z_{s=s_i}\,(s) \qquad \text{A8}$$

The position of the beginning of the primary phase s_1 is defined as the intersection of equations B6 and B7 when $e^{s_1}\ is$ small i.e. $C_1 + e^{s_1} \approx C_1$, and $\frac{e^{s_1}}{C_1} \approx 0$

$$s_1 \approx 2 - log(C_1) \qquad \text{A.9}$$

$$S(s_1) \approx S_f \frac{e^{-2}}{1 + e^{-2}} = 0.12\, S_f \qquad \text{A.10}$$

The position of the end of the primary swelling s_2 is approximated with $e^{s_2} + C_1 \approx e^{s_2}$ and, $\frac{C_1}{e^{s_i}} \approx 0$

$$s_2 \approx 2 + log(C_1) \qquad \text{A.11}$$

$$S(s_2) \approx S_f \frac{e^2}{1+e^2} = 0.88\, S_f \qquad \text{A.12}$$

Note that $S(s_1)$ and $S(s_2)$ are independent of C_1.

A.3: How to Find the Theoretical Breaking Point of the Swelling Curve:

It is the minimum of the curve in equation A3:

Taking the third derivative:

$$S'''(s) = S_f C_1 e^s \frac{e^{2s} - 4C_1 e^s + C_1^2}{(C_1 + e^s)^4} \qquad \text{A.13}$$

Solving for $S'''(s) = 0$, gives the location of the breaking point:

$$s = log\left(C_1\left(2 + \sqrt{3}\right)\right) \qquad \text{A14}$$

$$S(s) = S_f \frac{2 + \sqrt{3}}{3 + \sqrt{3}} = 0.79\, S_f$$

Note that $S(s)$ is independent of C_1.

A.4: How to Find the Approximate Limits between Primary and Secondary Swelling (Other Method):

Consider the straight line from the inflection point to this time at $s = log(C_1)$ and amplitude $\frac{S_f}{2}$ to the end of the experiment at $s = log(t_{end})$ and amplitude S_f

$$L(s) = \frac{S_f}{2(log(t_{end}) - log(C_1))}(log(t_{end}) - 2\, log(C_1) + \ \ s)$$

$$L(s) \in [0, S_f]$$

$$s > log(t_{end}) - 2log\ (C_1)$$

$$s < log(t_{end})$$

The two points of maximum curvature can be found by solving the following equation:

$$L'(s) \approx S'(s)$$

$$\frac{1}{2\,log\left(\frac{t_{end}}{C_1}\right)} \approx \frac{e^s}{(C_1 + e^s)^2}$$

$$e^{2s} + C_1^2 + 2e^s(C_1 - \ log\ (\tfrac{t_{end}}{C_1})) = 0$$

Posing:

$$A = C_1 - log\left(\frac{t_{end}}{C_1}\right)$$

The equation becomes:

$$e^{2s} + C_2^2 + 2A\,e^s = 0$$

Solutions:

$$s = log\ (-A \pm \sqrt{A^2 - C_1^2}$$

Explicit solutions:

$$s \approx log\left(-C_1 + log\left(\frac{t_{end}}{C_1}\right) \pm \sqrt{\log\left(\frac{t_{end}}{C_1}\right)\left(log\left(\frac{t_{end}}{C_1}\right) - 2\,C_1\right)}\right)$$

This corresponds to the two points of the limits of primary and secondary swelling.

Appendix B:

Parameters of the Model: $S(s) = S_f \frac{e^s}{(C_1+e^s)}$

B.1. How to Find the Parameter C_1 from Equation (1) using the Test Data at the Breaking Point Coordinates

Starting with equation (1) in the main text:

$$S(s) = S_f \frac{e^s}{C_1+e^s} \qquad \text{B1}$$

Inserting the observed break point at the time t_b and swelling amplitude S_b:

$$S_b = S(s_b) = S_f \frac{e^{s_b}}{C_1+e^{s_b}} \qquad \text{B2}$$

with $t_b = e^{s_b}$

The parameter C_1 can be derived:

$$C_1 = \frac{(S_f - S_b)\, t_b}{S_b} \qquad \text{B3}$$

B.2 How to Find the Parameters C_{21}, C_{22}, w_2, C_{11}, C_{12}, and w_1 from Equations 2-3 and 5-6

Taking the values of swelling at S_b and S_{end} and computing the slope:

$$C_{22} = \frac{S_{end} - S_b}{s_{end} - s_{end}} \qquad \text{B4}$$

Computing the interception of the line on the Y-axis:

$$C_{21} = S_{end} - C_{22} s_{end} \qquad \text{B5}$$

Draw the line between the breaking point s_b and ending value s_{end}:

$$S_{22} = C_{21} + C_{22} s \qquad \text{B6}$$

The parameter w_2 is determined by adjustment or visually in comparing the test data with the two model curves of equations A1 and A6.

The same procedure is used to determine C_{11}, C_{12} and w_1 if needed.

Supplementary Files

This is a list of supplementary files associated with this preprint. Click to download.

- AppendixA.docx